Content of supporting information:

S1. Additional experimental details

S1.1. Zeolite Samples

Zeolite H-MFI(29) was obtained commercially from Conteka/Zeolyst in the H-form (crystal size ~ 100 nm forming aggregates of 0.6 µm). Zeolite FER(9) was obtained from Tosoh in the K^+ form (HSZ 720KOA). It is converted to NH_4^+ form using 0.1M solution of NH_4Cl. The exchange process with NH_4^+ ions was repeated for 3 times during 4 h at 353K under agitation. The catalyst was centrifuged two times during 20 mins after each exchange. The catalyst paste obtained is then dried in air at 373K overnight. The sample was calcined at 773K for 5 h (heating ramp of 2K min^{-1}) in flowing air (Air Liquide) and cooled at room temperature with the same ramp to obtain the H-form of the zeolite. Zeolite TON(38) was kindly supplied by RIPP, Beijing, China and used as a parent sample in the work by Verboekend et al. [1] The sample was heated at 823K for 15 h (heating ramp of 3K min^{-1}) to remove the organic template. The zeolite sample is then converted to H-form using an ion exchange process as described above for FER. Zeolite H-CHA(13) was synthesized in our laboratory using a standard synthesis procedures. [2]

S1.2. Catalytic Testing

A self-supported pellet (about 20 mg with surface area of 2 cm^2) was placed into a transmission IR *Operando* reactor-cell and activated at 750K in a nitrogen-oxygen flow (95% N_2 and 5% O_2) for 5 hours. The characteristic absorption coefficients of the acidic OH groups (band at 3600 cm^{-1}) of the zeolites were determined by volumetric titration method using accurate doses of pyridine or ammonia (See Table S1). The monomolecular cracking of propane and n-butane (Air Liquide) was performed over all zeolites mentioned above at temperature range 580-710 K under atmospheric pressure. The data for propane and

n-butane cracking over MFI(29) were taken from our previous work.[3] The partial pressures of alkanes were adjusted by the dilution in N_2 gas (Air Liquide). The product analysis was done by online gas phase chromatography (HP 3800), equipped with FID detector with an alumina column (KCl/Al_2O_3, 30 m length, 350 µm internal diameter). No hydrocarbons with longer chain length than reactant or deactivation of the catalyst were observed because of very low total conversion limit (below 0.5%). The apparent cracking rates (r_{app}) were obtained by equation S1 below.[4]

$$r_{\mathrm{app}} = \frac{F}{W} \sum_{i=1}^{n-2} y_i \qquad \text{S1}$$

Where, *F*, *W* and *y* are the molar flow rate of alkane reactant, mass of the catalyst and molar yields of lower alkanes (i carbon atoms) respectively.

It must be mentioned here that the rate measurements are not affected by the geometry of the operando cell.[3] The key aspect of the present work was to record the IR spectra of the zeolite acidic OH groups perturbed by the interaction with the hydrocarbons at reaction conditions with simultaneous rate measurements. Nicolet 6700 FT-IR instrument with MCT detector at 4 cm^{-1} resolution was used for IR analysis. The quantification of number of hydrocarbon molecules interacted with Brønsted acid OH groups was done by subtracting the IR spectrum of the bare activated zeolite from the IR spectra recorded during the reaction (at certain temperature and pressure). The difference spectra obtained is then corrected for the gas phase alkane in the reactor-cell and water in the spectrometer. The decrease in νOH band intensity (*I*) due to hydrocarbon adsorption was fully reversible and the initial intensity of νOH band was fully restored after shutting off the reactant flow ascertaining the absence of irreversible poisoning of the active acid sites during the reaction (See Figure 1 in the main article). Therefore the confident determination of the concentration of the acid sites interacting with the alkane reactant $[\mathrm{ZOH} \ldots \mathrm{A}]$ can be done using the integrated intensity *I* of the difference spectra (negative band at 3600 cm^{-1}) and the absorption coefficient ϵ_{OH} using

$$[ZOH \ldots A] = \frac{IS}{\epsilon_{OH}\, W} \qquad \text{S2}$$

Where, *S* and *W* are the geometric surface are and the mass of the pellet, respectively.

ϵ_{OH} is obtained by monitoring the decrease of the νOH band area characteristic of the acidic OH groups (band at 3600 cm^{-1}) upon exposure to accurate doses of probe molecule (pyridine/ammonia) which results from the protonation of the probe molecule by these acidic OH groups (ZOH + $Py/NH_3 \rightarrow ZO^{-}\cdots PyH^{+}/NH_4^{+}$). The slope of the curve of the νOH area versus amount of adsorbed probe molecule yielded a εOH values listed in Table S1 below (See Figure S1). To be consistent, the total numbers of Brønsted acid groups (ZOH) were also determined in the same experiment. [3]

Table S1. Characteristics of zeolite samples

Zeolite	Source	Framework Si/Al ratio	Brønsted acid sites (µmol g^{-1})	Lewis acid sites (µmol g^{-1})	ε_{OH} (cm µmol^{-1})	µporous Surface Area (m^2/g)	µporous volume (cm^3 g^{-1})
MFI*	CBV 5020 (Zeolyst)	29	380	30	3.5 ± 0.2	454	0.192
FER	HSZ-720KOA (Tosoh)	9	852	-	4.05 ± 0.2[5]	170	-
TON[1]*	RIPP, Beijing, China	38	208	27	3.2 ± 0.03	227	0.08
CHA#	synthesized	13	1027	15	4.55 ± 0.1	141	0.0078

* Py and # NH_3 as probe molecules

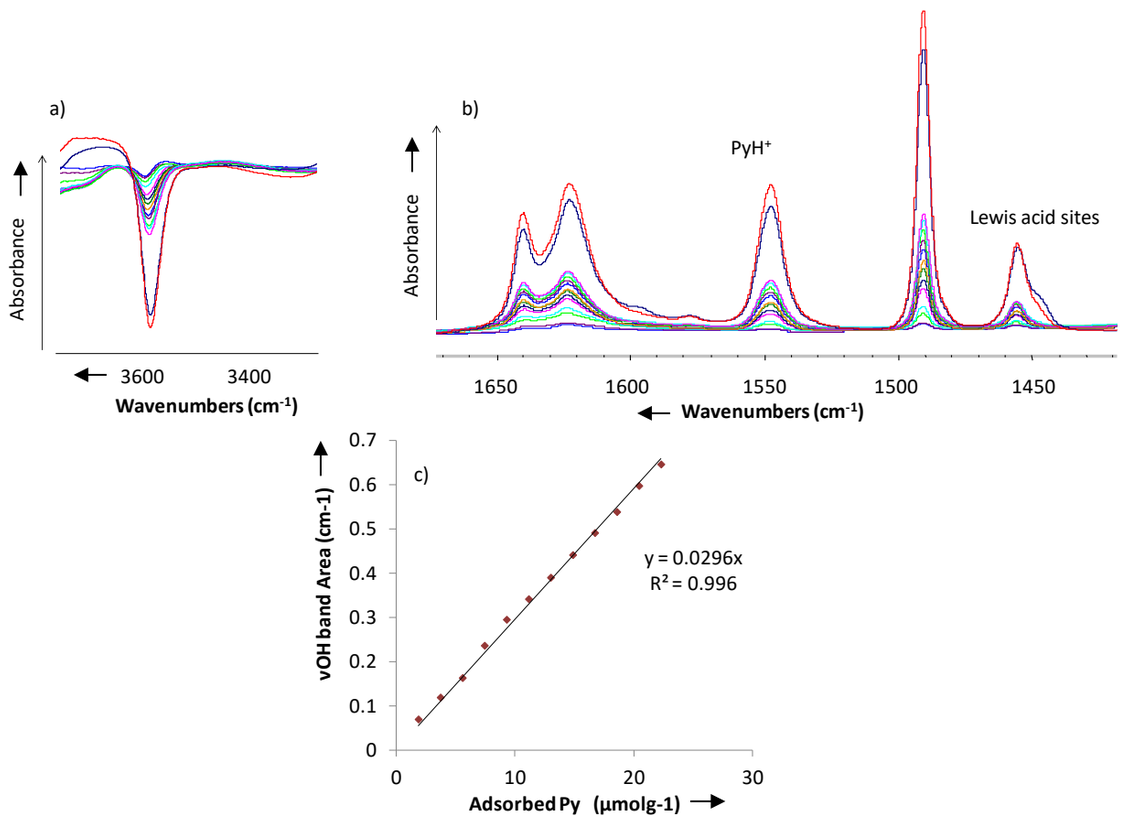

Figure S1 a). The subtracted spectra of H-TON(38) after successive addition of pyridine in the vOH range (band at 3600 cm^{-1}), b). The spectra of H-TON(38) showing the pyridinium ring vibration and c). Dependence of the acidic OH groups on the concentration of adsorbed pyridine.

S1.3. ^{27}Al MAS NMR spectroscopy of zeolite samples

^{27}Al MAS NMR spectra were collected on Bruker Avance 500 MHz spectrometer in a narrow bore 11.7 Tesla magnet at 130.287 MHz using 4 mm probe with a magic angle spinning rate of 12 kHz. ^{27}Al NMR spectra were recorded at ambient temperature by averaging 4096 scans with 2.33 µs pulse and a 0.5 s delay. These spectra are shown in Figure S2. The ^{27}Al NMR spectra of TON, CHA and FER shows the presence of peak at 0 ppm confirming the presence of extra-framework Al species.

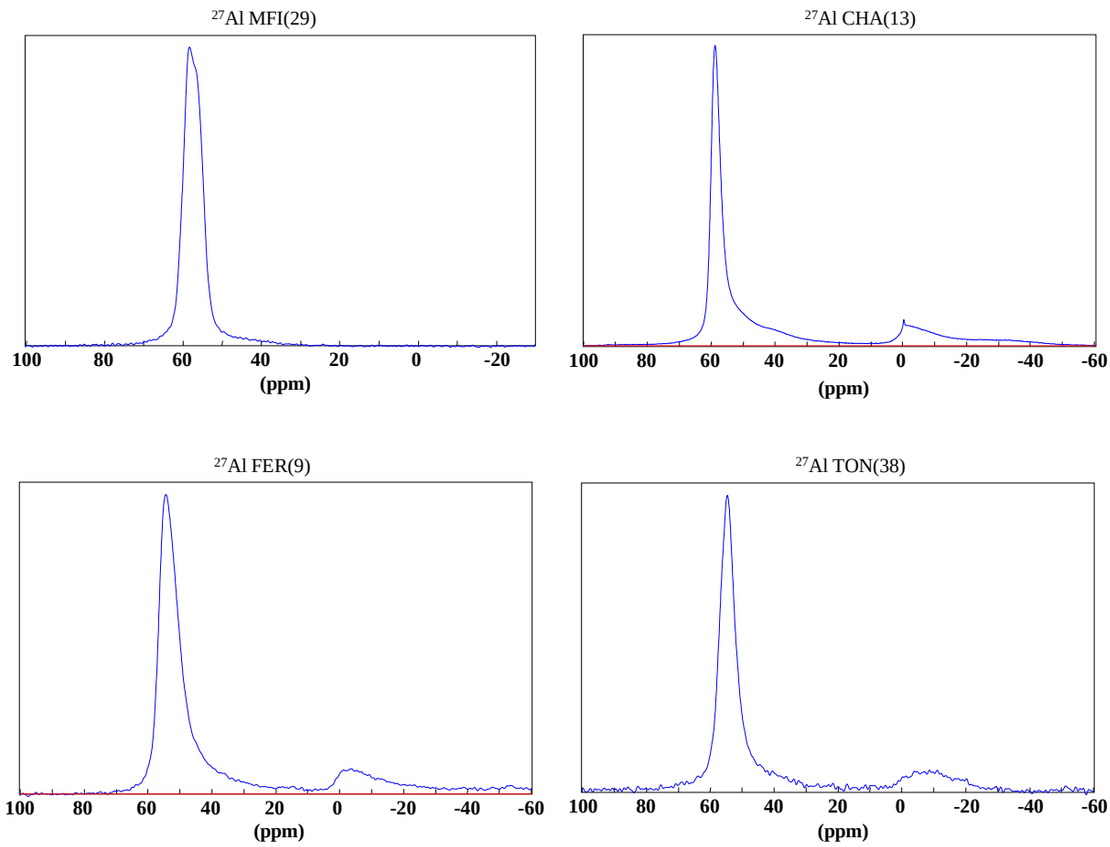

Figure S2. ^{27}Al MAS NMR spectra of all zeolite samples

S2. Adsorption isotherms, van't Hoff plots and reliability of adsorption parameters.

Figure S3a and S3b show the adsorption isotherms while Figure S3c shows corresponding van't Hoff plots obtained for propane and n-butane adsorption over all zeolites. The coverage of acid sites increased linearly with the alkane pressure, indicating that, within the pressure and temperature ranges reported here, alkane adsorption obeyed Henry's law.

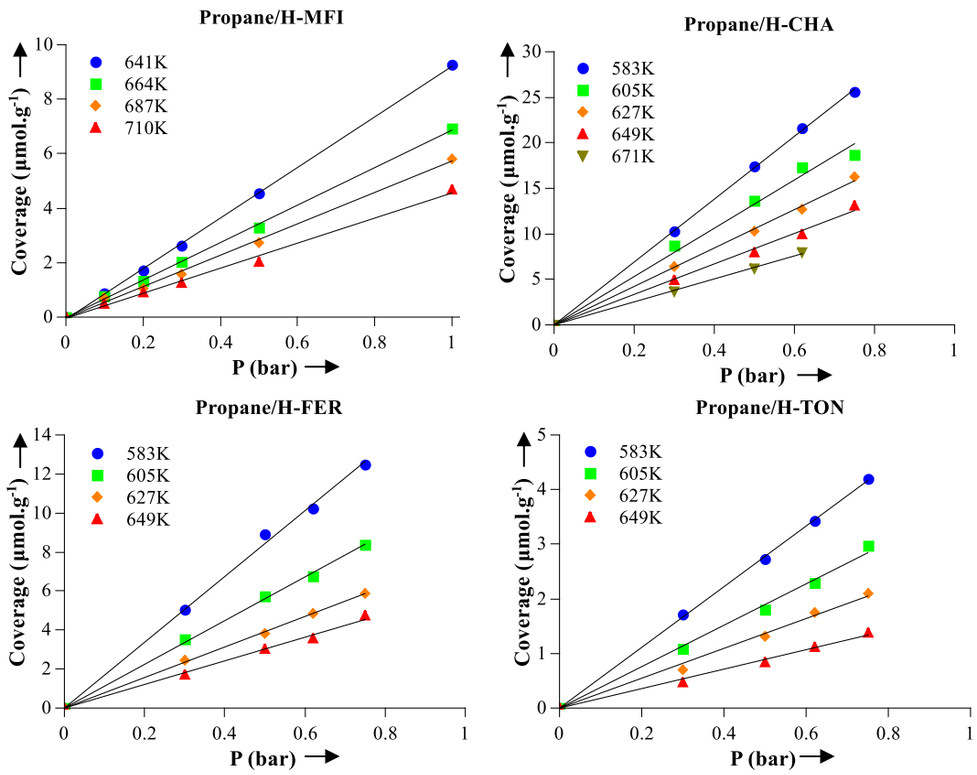

Figure S3a. Adsorption isotherms for propane/Zeolite

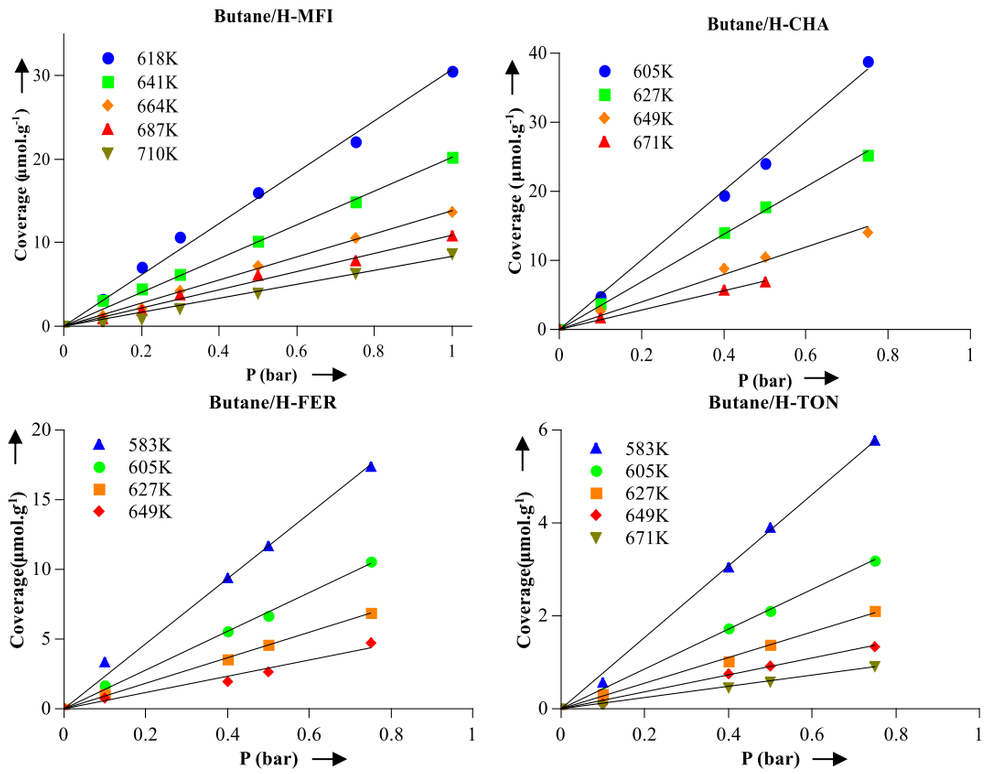

Figure S3b. Adsorption isotherms for n-butane/Zeolite

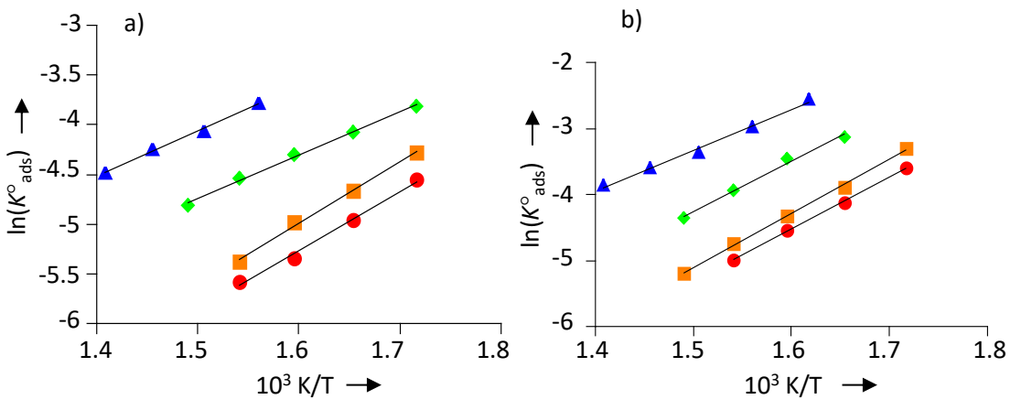

Figure S3c. van't Hoff plots of a) propane and b) n-butane adsorption over zeolites; MFI (▲), CHA (◆), TON (■), FER (●)

S2.1 Error analysis of adsorption parameters

The determination of adsorption enthalpy relies on the estimates of the concentration of hydrogen bonded complexes $[ZOH \cdots A]$ as follows:

$$\Delta_{ads}H = -R\frac{\partial K^{\circ}_{ads}}{\partial T^{-1}} = -\frac{RP^{\circ}}{[ZOH]_0}\frac{\partial^2[ZOH \cdots A]}{\partial T^{-1}\,\partial P} \qquad \text{S3}$$

Where the derivatives with respect to P and T^{-1} are actually obtained by linear regression of the adsorption isotherms (Figs S3a and S3b) and of the van't Hoff plots (Fig. S3c), respectively. The concentration of hydrogen bonded complexes $[ZOH \cdots A]$ is obtained by Equation S2. Hence:

$$\Delta_{ads}H = -\frac{RP^{\circ}S}{[ZOH]_0\,\epsilon_0\,W}\frac{\partial^2 I}{\partial T^{-1}\,\partial P} \qquad \text{S4}$$

Random errors and in the determination of the integrated intensity I of the OH band are thus included in the standard error of the linear regression given in Table 1. Systematic offsets error on the integrated intensity *I* would cancel out in the linear regressions. On the other hand, errors on the absorption coefficient ϵ_0 and total amount of acid sites $[ZOH]_0$ directly impact the error on the adsorption enthalpy $\Delta_{ads}H$. Table 1 of the main text shows that the values obtained in the present work differ by less than 15% from previous determinations based on calorimetry (maximum absolute deviation: 8 kJ mol^{-1}) and for which no confidence interval is reported.

The adsorption entropy is determined from the linear regression of the van't Hoff plots. Hence:

$$\Delta_{ads}S = R\,\langle \ln K_{ads} \rangle - \Delta_{ads}H\,\langle \frac{1}{T} \rangle \qquad \text{S5}$$

where the brackets denote the mean of the experimental values. As shown by this expression, random errors on $[ZOH \cdots A]$ are minimized by the averaging and even a major systematic error on these values have a limited impact. Hence, a very large systematic error in the coverage of ~ 20% would affect the entropies by $\sim R\,ln\,(1.2) \sim 1.5$ J mol^{-1} K^{-1} which is well within the confidence intervals ($\pm$ 2 standard error). The second source of error is the error on $\Delta_{ads}H$ discussed above. Using a conservative value of ~ 10 kJ mol^{-1} for the error on $\Delta_{ads}H$, this would yield 16 J mol^{-1} K^{-1} for the error in the adsorption entropy. Table 1 of the main paper shows that the values of $\Delta_{ads}H$ obtained in the present work differ on by less than 15% from previous calorimetric determinations (maximum absolute deviation: 16 J mol^{-1} K^{-1}), which is fully consistent with the present analysis.

S2.2 Adsorption parameters determined at low temperature (398 – 435K)

In order to validate the methodology and to determine whether the chosen temperature range would affect these values, complementary adsorption experiments were performed using a similar Operando cell at lower temperatures (398 – 435K). The values obtained are compared with those obtained at higher temperature for Propane in Table S2 and are in very good agreement.

Table S2. Adsorption parameters derived at low temperature range (398 – 435K)

Alkane/Zeolite	$\Delta_{ads}H$ (High T 583-710K)	$\Delta_{ads}S$ (High T 583-710K)	ΔH_{ads} (Low T 398-435K)	ΔS_{ads} (Low T 398-435K)
C3/MFI	-38(2)	-91(3)	-39(1)	-92(1)
C3/FER	-49(2)	-117(4)	-47(2)	-117(4)
C3/CHA	-36(1)	-93(2)	-36(1)	-86(2)

S3. Estimation of Effective pore radii

In this work, we have used the effective pore diameter calculated by averaging the minor and major axes of the elliptical channel after considering the oxygen atom diameter (2.7 Å)[6]. For example, the effective pore radii of the 8MR (3.5 x 4.8 Å) and 10MR (4.2 x 5.4 Å) channels in FER are 3.4 Å and 3.7 Å respectively. Similarly, the effective pore radius of MFI intersection (6.3 x 7.0 Å) and CHA cage (6.7 x 7.0 Å) is 4.6 Å.

S4. Apparent rate (r_{app}) versus coverage plots

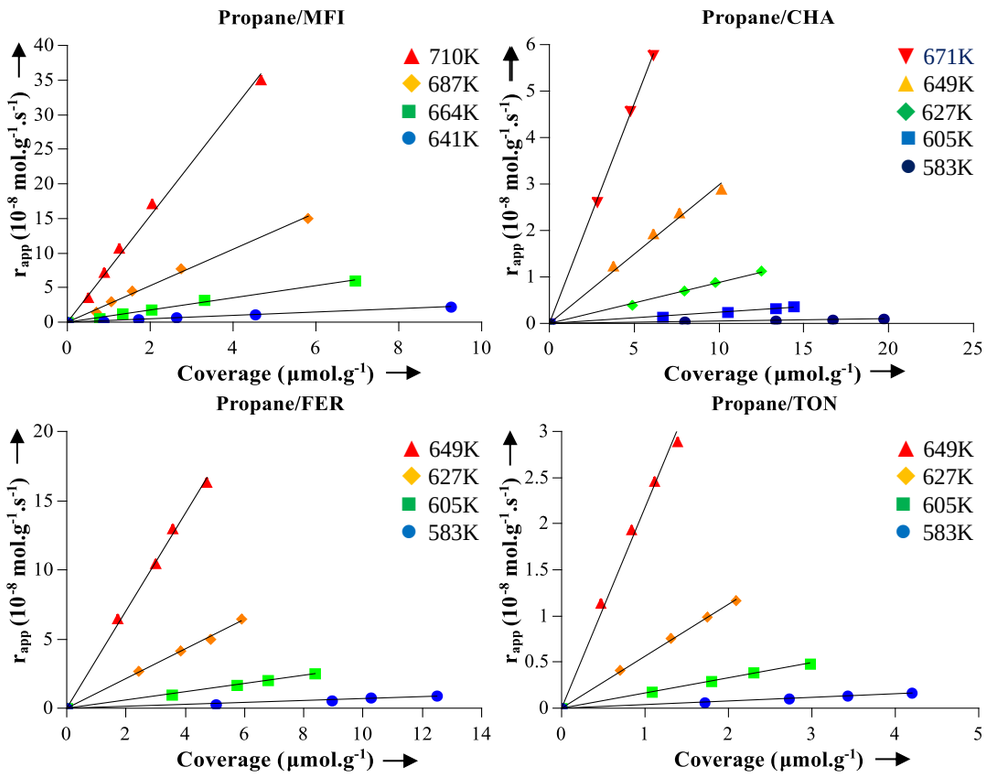

Figure S4a. Apparent cracking rates (r_{app}) versus concentration of acid site-alkane hydrogen bond complexes (coverage) for propane monomolecular cracking over MFI, CHA, FER and TON zeolites at various temperatures.

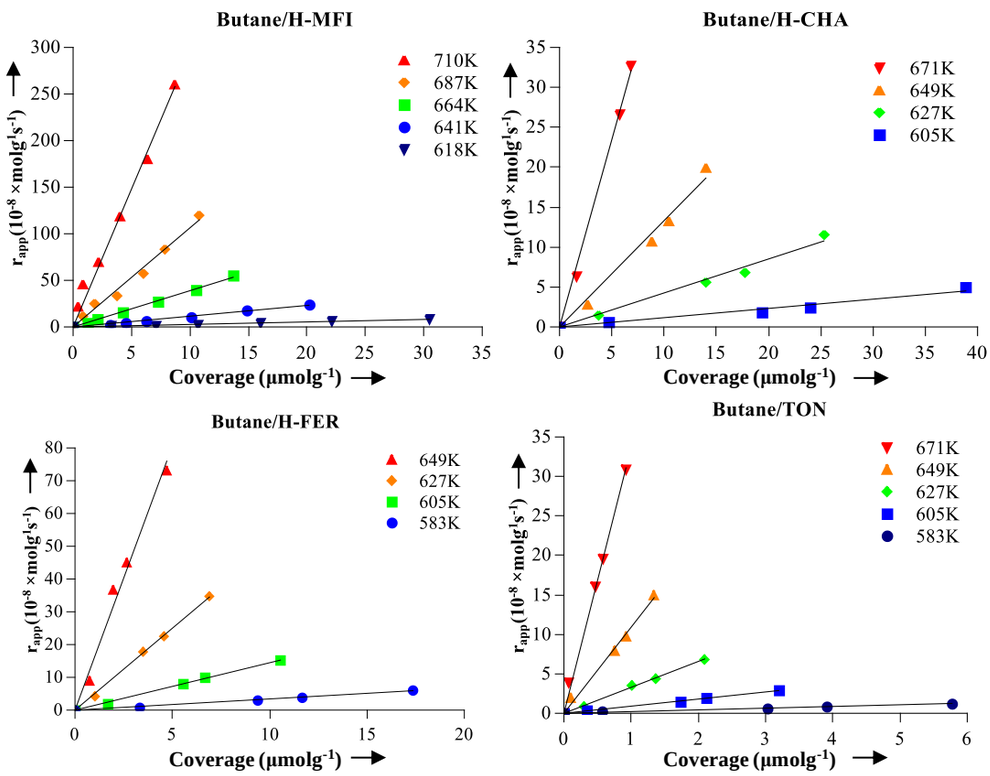

Figure S4b. Apparent cracking rates (r_{app}) versus concentration of acid site-alkane hydrogen complexes for n-butane monomolecular cracking over MFI, CHA, FER and TON zeolites at various temperatures.

S5. Statistical significance tests on Arrhenius parameters

The value of the intrinsic cracking rate constant (k_{int}) depends on temperature (T), the nature of the alkane molecule (mol) and the type of zeolite (Cat). ν is the universal frequency factor.

The standard transition state theory allows expressing the intrinsic rate constant as

$$k_{int}(T, mol, Cat) = \nu \, exp\left(\frac{\Delta S^{\ddagger}}{R}\right) exp\left(\frac{-E_a}{RT}\right) \quad \text{S6}$$

Where $\nu = ek_BT/h$ is independent of the nature of the alkane/zeolite system.

Taking natural log of both sides divided by ν yields:

$$\ln\left(\frac{k(T, mol, Cat)}{\nu}\right) = \frac{\Delta S^{\ddagger}}{R} - \frac{E_a}{R}\left(\frac{1}{T}\right) \quad \text{S7}$$

Equation S7 is a particular form of the linearized Arrhenius equation generally used to derive activation energies and entropies. This equation is linear with respect to 1/T and the corresponding coefficients multiplied by R yields activation energy (E_a) and activation entropy ($\Delta S^{\ddagger}$). Classically, this relationship would be used for each (alkane, zeolite) system in order to determine the particular values of activation parameters corresponding to each system. In this unrestricted model (Model 1), both activation energy and activation entropy are expected to depend on the alkane and zeolite type. Denoting intercept and slope are as β_0 and β_1, respectively yields:

Model 1: $$\ln\left(\frac{k(T, mol, Cat)}{\nu}\right) = \beta_0\,(mol, Cat) + \beta_1(mol, Cat)\frac{1}{T}$$

Using this approach, the values obtained for activation energies are found to lie in a narrow range (185-190 kJ mol^{-1}, see Table S3a below) while those for activation entropies show a much larger variability (-15 to +12 J mol^{-1} K^{-1}, Table S3a below).

To test whether the small differences in activation energy are statistically significant, a restricted linear model (Model 2) nested within Model 1 can be built. Assuming that only intercept β_0 (hence activation entropy $\Delta S^{\ddagger}$) depends on the molecule and on the catalyst while the slope (hence activation energy) is constant for all the systems studied yields:

Model 2: $$\ln\left(\frac{k(T, mol, Cat)}{\nu}\right) = \beta_0\,(mol, Cat) + \beta_1\frac{1}{T}$$

Typically Model 1 (16 parameters with 141 observations) would provide better fit to the data than Model 2 (9 parameters with 141 observations). However, the additional parameters of Model 1 might lead to an overfit of the data and both models must be compared on statistical grounds. This was done using an F-test to test the null-hypothesis H_0 that the simpler model (Model 2) is sufficient to fit the data compared to the full model (Model 1). The probability to reject the null-hypothesis (p-value) was found to be 0.36, which is greater than the usual significant level (p = 0.05) and allowed concluding that the null-hypothesis cannot be rejected. Hence, Model 2 describes adequately the present data.

Table S3a and S3b shows the activation energies and entropies obtained using both models along with their standard errors in parenthesis for all systems investigated.

Table S3a. Activation energies obtained using both Models along with the standard errors

	MFI		CHA	
	Model 2	Model 1	Model 2	Model 1
C3	187(1)	189(1)	187(1)	190(1)
C4	187(1)	186(1)	187(1)	187(2)
	FER		TON	
	Model 2	Model 1	Model 2	Model 1
C3	187(1)	186(1)	187(1)	187(1)
C4	187(1)	185(1)	187(1)	186(1)

E_a reported in $kJmol^{-1}$

Table S3b. Activation entropies obtained using both Models along with the standard errors

	MFI		CHA	
	Model 2	Model 1	Model 2	Model 1
C3	-18(1)	-15(1)	-19(1)	-14(1)
C4	-5(1)	-7(1)	-6(1)	-6(2)
	FER		TON	
	Model 2	Model 1	Model 2	Model 1
C3	2(2)	0(1)	-3(2)	-3(1)
C4	12(2)	12(1)	10(2)	11(1)

$\Delta S^{\ddagger}$ reported in $JK^{-1}mol^{-1}$

Figure S5 shows the Arrhenius plots for propane and n-butane over all zeolites using the experimental data points along with the predicted intrinsic rate coefficients obtained by using Model 1 and Model 2.

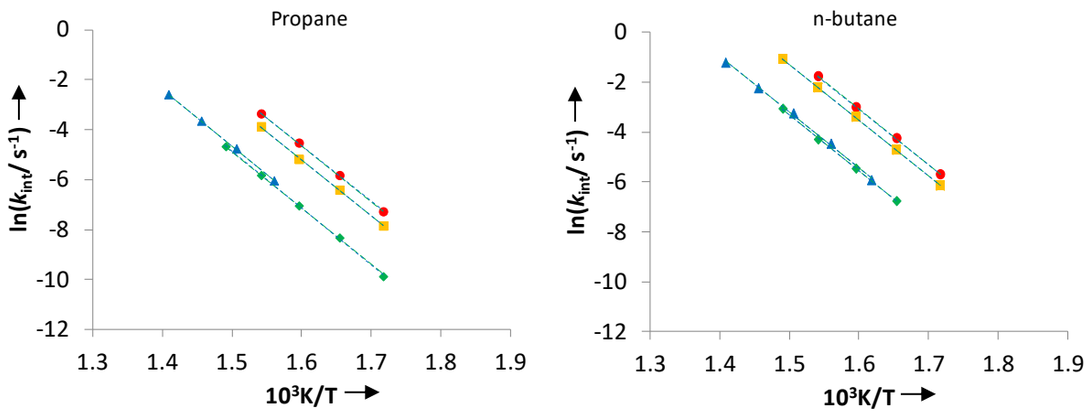

Figure S5. Arrhenius plots for propane and n-butane over all zeolites with experimental data (solid points; MFI (▲), CHA (◆), TON (■), FER (●)) and the predicted intrinsic rate coefficients using Model 2(Green dotted line– –) and Model 1(Blue dotted line --).

S6. Waterfall chart for butane:

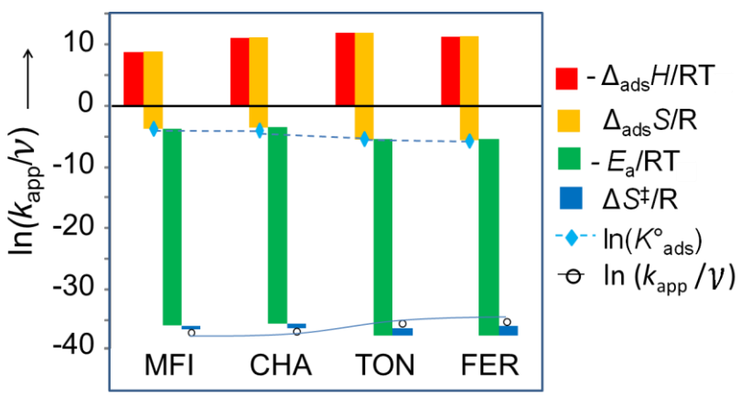

Figure S6. Waterfall plot of the adsorption and kinetic terms contributing to the adsorption constant and apparent rate constant for n- butane at T = 700K

S7. Absolute entropies at the adsorbed and transition states

The absolute values of the gas phase entropies for propane and butane were taken directly from the ref [7] at 700K. The absolute values of entropies at the adsorbed (S_{ads}) and transition state ($S^{‡}$) were calculated as follows:

$$S_{ads} = S^{\circ}_{(g)} + \Delta S_{ads} \quad \text{S8}$$

$$S^{‡} = S_{ads} + \Delta S^{‡} \quad \text{S9}$$

Table S4. Absolute entropies at the adsorbed and transition state (Entropies reported in $Jmol^{-1}K^{-1}$)

Zeolites	Propane $S^{\circ}_{(g)} = 361$		Butane $S^{\circ}_{(g)} = 429$	
	S_{ads}	$S^{‡}$	S_{ads}	$S^{‡}$
MFI	270	252	324	319
CHA	268	249	306	300
TON	242	239	284	294
FER	244	246	287	299

S8. References

[1] D. Verboekend, K. Thomas, M. Milina, S. Mitchell, J. Perez-Ramirez, J.-P. Gilson, *Catal. Sci. Technol.* **2011**, *1*, 1331.

[2] H. Robson, *Verified Synthesis of Zeolitic Materials: Second Edition*, Elsevier Science, **2001**.

[3] H. Li, S. A. Kadam, A. Vimont, R. F. Wormsbecher, A. Travert, *ACS Catal.* **2016**, *6*, 4536.

[4] T. F. Narbeshuber, H. Vinek, J. A. Lercher, *J. Catal.* **1995**, *157*, 388.

[5] B. Wichterlova, Z. Tvaruzkova, Z. Sobalık, P. Sarv, *Microporous Mesoporous Mater.* **1998**, *24*, 222.

[6] R. Gounder, E. Iglesia, *J. Am. Chem. Soc.* **2009**, *131*, 1958.

[7] P. Vansteenkiste, V. Van Speybroeck, G. B. Marin, M. Waroquier, *The Journal of Physical Chemistry A* **2003**, *107*, 3139.